RASONIC IMAGING 13, 347-359 (1991)

IMPROVED RESOLUTION BACKSCATTER COEFFICIENT IMAGING

Evan J. Boote,[1] Timothy J. Hall,[2]
Ernest L. Madsen and James A. Zagzebski

Department of Medical Physics
University of Wisconsin
Madison, WI 53706

This paper reports the extension of a method for imaging acoustic backscatter coefficients that allows for greater spatial resolution in the resulting images. This is done by using a broad-band excitation pulse and short-duration time gates in the analysis. The images produced had better spatial resolution than the previously reported technique [Ultrasonic Imaging 10, 121-138]. Furthermore, the pixel values were based upon quantitatively accurate backscatter coefficients at given spatial locations. The paper also discusses the additional computational requirements of greater spatial resolution and proposes a least-squares fit to a smoothly varying set of sparse data to generate the data points in between.

Key words: Backscatter coefficient; quantitative imaging, tissue characterization, ultrasound.

INTRODUCTION

Backscatter coefficient imaging, initially proposed by O'Donnell [1,2] and more recently studied by our group [3], is the spatial mapping to gray scale images of acoustic backscatter coefficients measured from a volume of tissue. O'Donnell's method involves the application of several assumptions and approximations; e.g. an impluse response function is introduced which depends on range but not on off-axis distance and is assumed to have a Gaussian distribution frequency content. Also, a canonical range-dependent beam area associated only with a center-frequency is assumed such that contributions to the received signal from identical scatterers within the area are treated equally. The images presented in our previous work [3] were produced using a method of data reduction [4] which accounts for tissue and instrumentation factors with a high level of rigor. These factors include the

---

[1]Present address: University of Missouri Hospital and Clinics, Department of Radiology, One Hospital Drive, Columbia, MO 65212.

[2]Present address: University of Kansas Medical Center, Department of Radiology, 39th and Rainbow Blvd, Kansas City, KS 66103.

0161-7346/91 $3.00

pulser/receiver electronics, the geometry of the piezoelectric element and the propagation of the beam through tissue. This method of analysis differs from integrated backscatter measurements in that backscatter coefficients are determined for a specific frequency rather than representing an average backscatter coefficient for a band of frequencies. While the images produced in the previous work were based on accurate backscatter coefficients determined for a set of spatial locations, these images had less than optimal spatial resolution in the axial direction. This was the due to the use of narrow-band pulses and relatively long duration time gates in the acquisition and analysis of the RF echo data. Resolution in the axial direction can be improved upon by using shorter (broad-band) pulses and shorter duration time gates.

When short duration, broad-banded pulses are applied, it becomes necessary to explicitly account for the frequency dependence of scattering in the data reduction in order to obtain accurate results [4,5,6]. This frequency dependence is unknown in tissue except for a few cases, prompting the suggestion of an iterating data analysis method for broadband pulses [4]. Alternatively, Hall [7] reports that accurate results from a broadband pulse (60% frequency bandwidth) experiment can be obtained using this technique under certain conditions *without explicitly accounting for the frequency dependence of scatter.* The conditions are a frequency spectrum that is symmetric about the center frequency and analysis of the data at or close to the center frequency of the pulse. These positive results spurred the utilization of broad-band, short-time-gate analysis in our application of backscatter coefficient imaging.

METHODS

In this study, echo signals were recorded while a pulsed transducer is translated linearly over several closely spaced scan planes. A typical echo signal waveform is depicted in figure 1. The phase and amplitude of the waveform are related to the position of the ultrasound transducer, the direction in which it is pointed, and the distribution of scatterers in the medium. We use the index m to denote the transducer position within scan plane n, and divide the echo signal waveform along the time axis into a number of equal, contiguous segments of duration τ with the axial position indicated by the index l. The backscatter coefficient at angular frequency ω_o corresponding to position (l′, m′ n′), is given by [3]

$$\eta_{l'm'n'}(\omega_o) \cong \frac{1}{(\Delta L+1)(\Delta M+1)(\Delta N+1)} * \sum_{l=l'-\frac{\Delta L}{2}}^{l'+\frac{\Delta L}{2}} \sum_{m=m'-\frac{\Delta M}{2}}^{m'+\frac{\Delta M}{2}} \sum_{n=n'-\frac{\Delta N}{2}}^{n'+\frac{\Delta N}{2}} \frac{\|V_s(\omega_o; l,m,n)\|^2}{a_l(\omega_o)} \quad (1)$$

where $V_S(\omega_0;l,m,n)$ is the Fourier transform at ω_0 (in this case, the center frequency of the acoustic pulse) of the echo voltage signal corresponding to the location (l, m, n) and $a_l(\omega_0)$ accounts for instrumental factors and attenuation in the medium. As Eq. (1) indicates, the backscatter coefficient at each location is obtained by averaging data over a three dimensional local neighborhood. ω_0 is the frequency for which the backscatter coefficient is determined and it may be any frequency within the bandpass of the transducer.

The derivation of Eq. (1) has been presented previously [3]. The denominator has the form

$$a_l(\omega_0) = \left(\frac{\tau}{2\pi}\right)^2 \iiint_{\Omega} d\vec{r} \left| \int_{-\infty}^{+\infty} d\omega\, T(\omega) B_0(\omega) \frac{g(\omega)}{g(\omega_0)} \operatorname{sinc}\left[\frac{(\omega-\omega_0)\tau}{2\pi}\right] [A_0(\vec{r},\omega)] \right|^2 \qquad (2)$$

where $B_0(\omega)$ is a set of complex coefficients corresponding to the superposition of continuous wave beams giving rise to the acoustic pulse. $T(\omega)$ is a force-to-voltage transfer function for the transducer and amplifiers. The product $T(\omega)B_0(\omega)$ is determined at the time of the experiment using an echo from a planar reflector as described by Madsen, et al[4]. Additional factors included in Eq. (2) [7] are $\| g(\omega) \|^2$, which represents the frequency dependence of the backscatter coefficient and $\| g(\omega_0) \|^2$ is the value of this function at the analysis frequency, ω_0. The volume Ω includes all scatterers that contribute to the signal over τ, the duration of the time gate. Introduction of the rectangular time gate leads to a convolution of frequencies, represented by the sinc function in Eq. (2). The term $A_0(\vec{r},\omega)$ describes the relative pressure distribution and has the form

$$A_0(\vec{r},\omega) = \iint_S ds\, \frac{e^{ik|\vec{r}-\vec{r}'|}}{|\vec{r}-\vec{r}'|}$$

where the integral is over the transducer surface S, $\vec{r}$ defines a point in the transducer field, $\vec{r}'$ terminates on area element ds on the transducer surface and k is the complex wavenumber.

When the durations of the acoustic pulse and time gate are large, a narrow bandwidth situation arises whereby $g(\omega)/g(\omega_0)$ is essentially unity over the range of frequencies contributing to the integral in Eq. (2); therefore, this ratio had been ignored in earlier tests of this method [4,5,7].

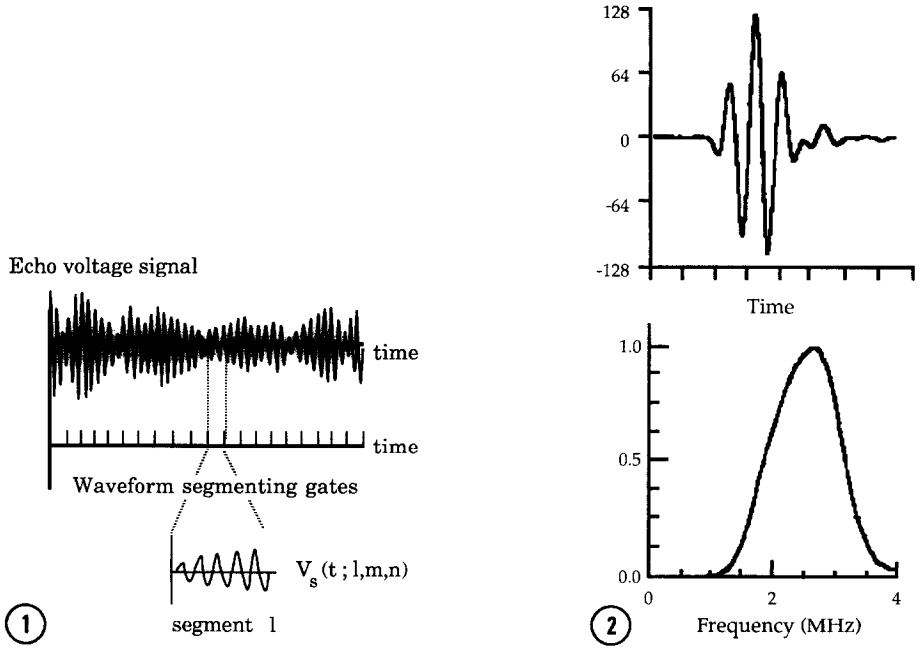

Fig. 1 A typical ultrasound echo signal waveform. In the data processing described, the signal is segmented into a number of gates and is assigned indices according to transducer position and gate depth (time).

Fig. 2 An echo signal from a reference reflector following a single cycle 2.5 MHz pulse on a 2.25 MHz transducer and the corresponding modulus of $T(\omega)B_O(\omega)$. After figure 8.1 of reference [7].

More recently, Hall [7] applied this data reduction method to several experimental situations. In one case, a broadband 2.5 MHz center frequency pulse was used to interrogate a gel phantom containing 59 μm mean particle diameter glass bead scatterers. A single cycle pulse at 2.5 MHz was amplified and applied to the transducer. The resulting echo signal from a reference reflector and the corresponding spectral content of this pulse are illustrated in figure 2. Data were analyzed assuming a simple power law form for the frequency dependence of scatter (i.e. $g(\omega)^2 \propto f^n$). Backscatter coefficients were determined for several analysis frequencies (ω_o) using varying gate durations and varying frequency dependence(n).

The results of Hall's experiment are shown in table I. The predicted backscatter coefficient (column 6) was computed using expressions derived by Faran [8]. Accurate results are obtained at the center frequency of the pulse (2.5 MHz) for 10, 2 and 0.5 μs gate durations, for any of the assumed frequency dependencies (column 1). However, for an analysis frequency of 2.0 MHz the accuracy of the experimental result assuming frequency independent scattering (n=0) decreases as shorter time-gates are employed. The same effect is noted for an analysis frequency of 3.0 MHz. When n=4, the assumed

Table I. Experimentally determined backscatter coefficients using different functional forms for the frequency dependence of scattering, for a pulse with a center frequency of 2.5 MHz. After table 8.1 of reference [7].

Assumed Frequency Dependence n	Analysis Frequency (MHz)	Backscatter coefficient x 10^5 cm^{-1} sr^{-1}			
		10 μs gate	2 μs gate	0.5 μs gate	Predicted
n=0	2.0	6.81 ± 0.93	7.60 ± 1.08	12.6 ± 1.5	5.63
	2.5	14.6 ± 1.7	16.0 ± 1.8	14.5 ± 1.7	13.2
	3.0	28.7 ± 4.0	23.1 ± 3.5	16.8 ± 1.9	25.8
n=2	2.0	6.71 ± 0.91	7.00 ± 0.99	9.13 ± 1.10	5.63
	2.5	14.7 ± 1.8	16.1 ± 1.8	15.0 ± 1.8	13.2
	3.0	29.2 ± 4.1	25.5 ± 3.8	23.1 ± 3.2	25.8
n=4	2.0	6.55 ± 0.89	6.20 ± 0.88	6.10 ± 0.74	5.63
	2.5	14.6 ± 1.8	15.9 ± 1.8	14.5 ± 1.7	13.2
	3.0	29.6 ± 4.1	27.3 ± 4.1	29.7 ± 3.4	25.8

frequency dependence is closer to the actual frequency dependence of scattering for 59 μm particles, and the results are in reasonable agreement for each of the gate durations and analysis frequencies. Moreover, the results at 2.5 MHz do not vary by more than 10% when the time-gate duration is changed or the assumed frequency dependence of the scattering is changed between n=0 to n=4 (Rayleigh scattering).

The lack of sensitivity to scattering frequency dependence at the center frequency of the pulse is likely due to $g(\omega)/g(\omega_0)$ vs. ω being nearly equal to unity for small increments from ω_0. In addition, the remainder of the integrand over ω in Eq. (2) is symmetric around ω_0. In this case, underestimates of the integrand for $\omega<\omega_0$ tend to be compensated for by overestimates of the integrand for $\omega>\omega_0$. Therefore, $g(\omega)/g(\omega_0)$ can be approximated by a function equal to unity when ω_0 is chosen at the center frequency. When ω_0 is not the center frequency, $g(\omega)/g(\omega_0)$ becomes a more important function in the integrand and the symmetry of the integrand around ω_0 no longer exists. Hence, a correct frequency dependence of scattering in the function $g(\omega)/g(\omega_0)$ is necessary for an accurate determination of the backscatter coefficient when ω_0 is chosen for a frequency off the center frequency.

EXPERIMENTAL PROTOCOL

In the present study, experiments reported in previous work [3] are essentially repeated, using the same transducers and phantoms as well as the

data collection protocol. Each phantom ultrasonically mimicks tissue both with respect to speed of sound and attenuation. One phantom contains cylindrical volumes with backscatter coefficients +3 dB and -3 dB with respect to the background; the other phantom has two spherical volumes (13 mm and 6 mm in diameter) which has a backscatter coefficient approximately -18 dB with respect to the background.

The transducers used are 2.25, 3.5 and 5 MHz, 19 mm aperture single element focused radiators. We departed from previous experimental technique by exciting each transducer with an amplified single cycle pulse at the center frequency, which produced a relatively broad frequency response as shown in figure 2. For each experiment, 75 to 100 waveforms of approximately 100 μs in duration were collected in 4 parallel planes, spaced 1 mm apart. Data analysis included evaluating Eq. (1) for each segment of the waveforms. This was performed in the previous manner [3], except instead of using 3 μs segments, 0.5 μs segments were used. The integral over frequency in Eq. (2) was evaluated using 121 frequencies spanning the bandwidth of the acoustic pulse. Since the analysis was performed at the center frequency of the spectrum, $g(\omega)/g(\omega_0)$ was set to unity over the entire range of ultrasonic frequencies.

RESULTS

Figures 3a, b, and c are backscatter coefficient images of a phantom with ± 3 dB scattering volumes (with respect to the backscatter coefficient of the background). Scans in figure 3a, b and c and subsequent data analysis were performed with center frequencies of 2.5, 3.5 and 5 MHz respectively. These are the center resonant frequencies for each of the transducers utilized in the study. Note the apparent improvement in the spatial resolution of these images compared to those for the same phantom in our previous report, shown in figures 4a, b and c.

Table II is a compilation of backscatter coefficients determined from three regions of interest on the images in figure 3. These regions correspond to the background and each area of backscatter contrast (± 3 dB with respect to the background). Table II also provides a comparison of these measured backscatter coefficients at each frequency with values predicted using the theory of Faran [8]. Note from the table that the images produced using the 0.5 μs gate analysis are quantitatively correct.

Figures 5a and b are images of a phantom with two spherical, low-scattering objects (referred to as phantom C in [3]). Figure 5c is a schematic diagram of this phantom. The two spherical objects are 13 mm in diameter and 6 mm in diameter. The data acquisition and analysis for the image in figure 5a utilized a 3 μs duration time gate; for the image in figure 5b, the data acquisition and analysis were identical except a 0.5 μs duration time gate was

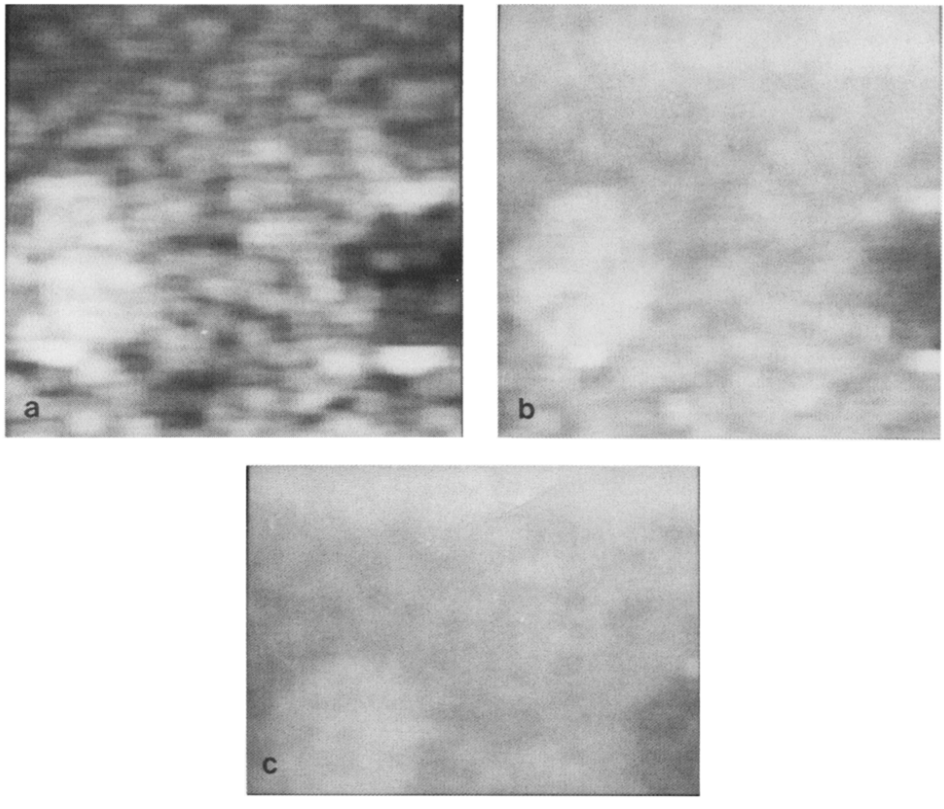

Fig. 3 Backscatter coefficient images of a phantom with +3 dB and -3 dB regions of contrast. In each case the transducer was excited with a single cycle pulse at the center frequency and analyzed with 0.5 μs rectangular gates. The analysis frequencies for the images are 2.5 MHz (a), 3.5 MHz (b), and 5 MHz (c).

employed. In figure 5a, the 6 mm sphere is not clearly resolved, while in figure 5b, the resolution of the 6 mm sphere is vastly improved. This demonstrates an improved high-contrast spatial resolution with the broad-band, short duration gate technique.

DISCUSSION

The method of data reduction used for computing backscatter coefficient images (Eqs. (1) through (3)) has been shown previously to provide accurate results in experiments using narrow frequency bandwidth conditions. This paper indicates that accurate results are obtained under experimental conditions using broad band frequency conditions and short (0.5 μs) time gates for analysis when the frequency of analysis is the center frequency of a symmetric pulse spectrum. These results hold even though there is no *a priori* knowledge of the frequency dependence of scattering.

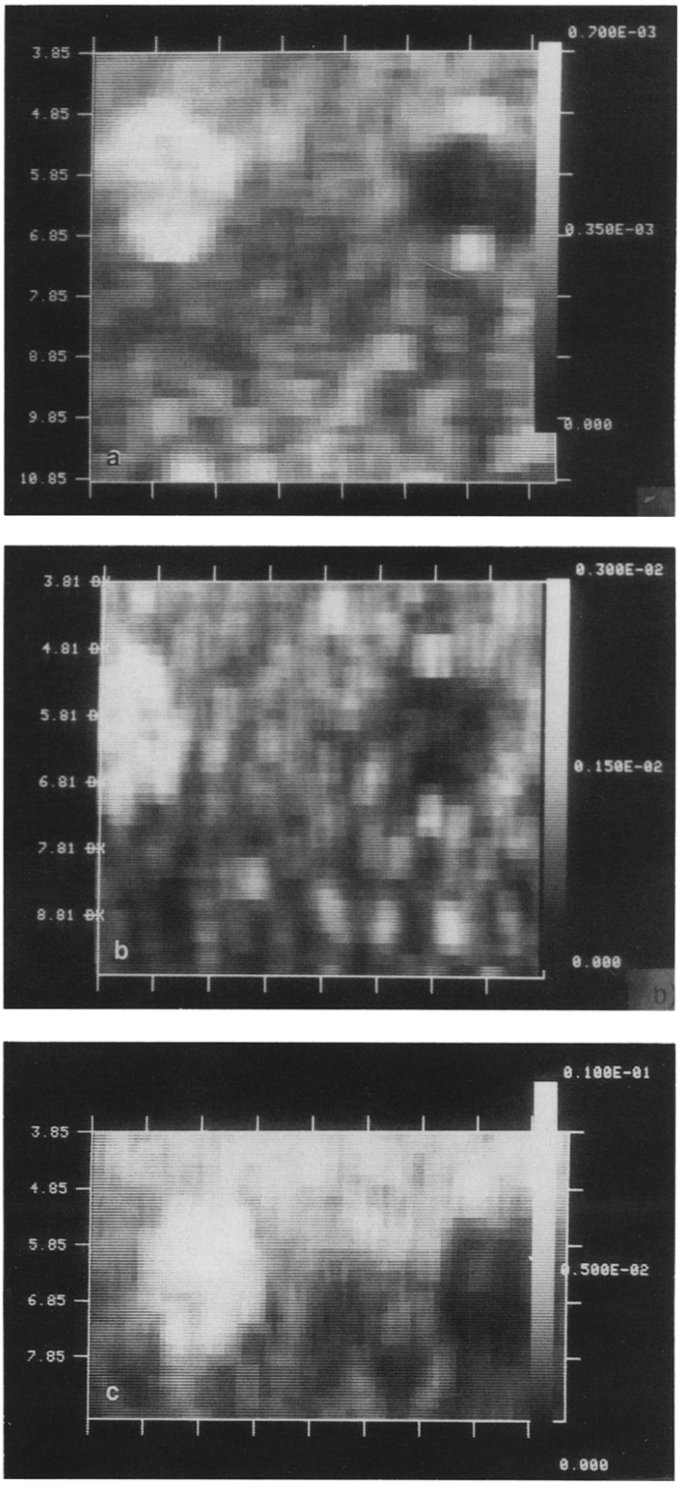

Fig. 4 Backscatter coefficient images of the same phantom shown in figure 3 except using a 3 μs tone burst at the center frequency and data analysis gates of 3 μs. The analysis frequencies for the images are 2.5 MHz (a), 3.5 MHz (b), and 5 MHz (c).

Table II. Experimentally determined backscatter coefficients from images depicted in figure 2 that have been acquired with a broadband pulse and analyzed with short duration time-gates. The predicted values are calculated using the theory of Faran [8].

Frequency ω_o (MHz)	Backscatter coefficient of background (cm^{-1} sr^{-1})		Backscatter coefficients in cylindrical volumes in dB relative to the background	
	Predicted	Experiment	-3 dB	+3 dB
2.5	2.8×10^{-4}	3.1×10^{-4}	-2.7	+3.5
3.5	9.5×10^{-4}	8.9×10^{-4}	-3.6	+2.9
5.0	3.1×10^{-3}	2.7×10^{-3}	-3.0	+2.8

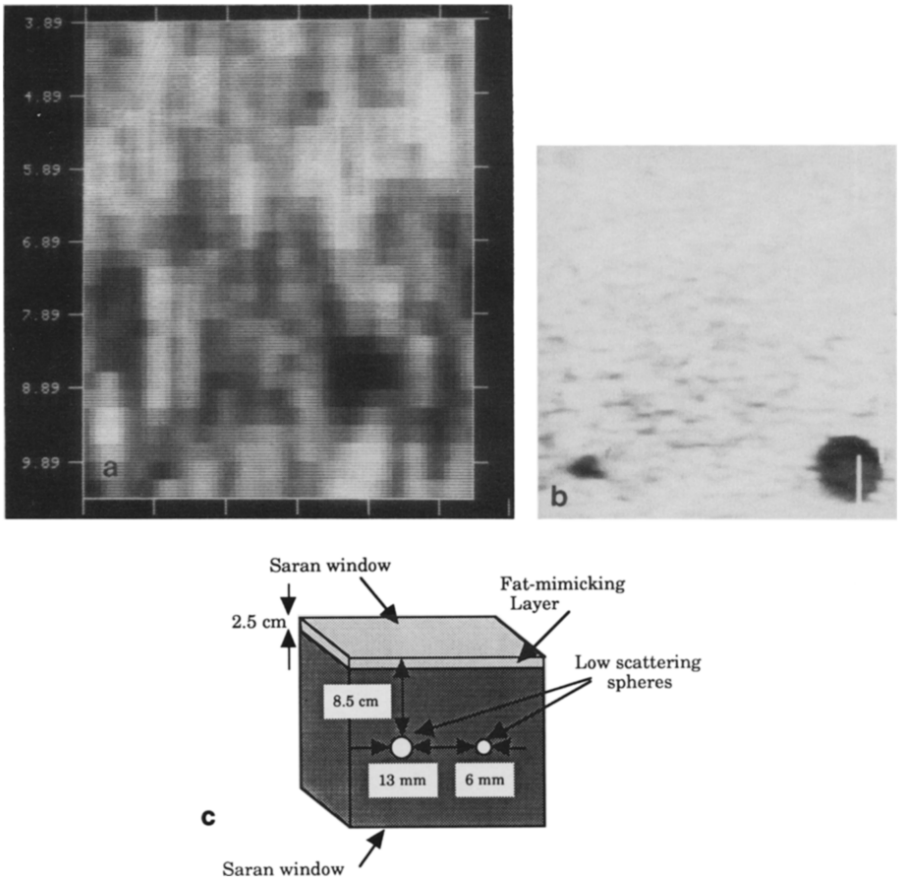

Fig. 5 Backscatter coefficient images of a phantom with two spherical, low-scattering objects. The data represented in (a) was analyzed with a 3 μs duration time gate while (b) utilized a 0.5 μs duration time gate.

(c) Tissue-mimicking phantom used in experiment producing images in figures a and b. The phantom has two low-scattering spheres embedded in the center of the phantom; one is 13 mm in diameter, the other is 6 mm in diameter.

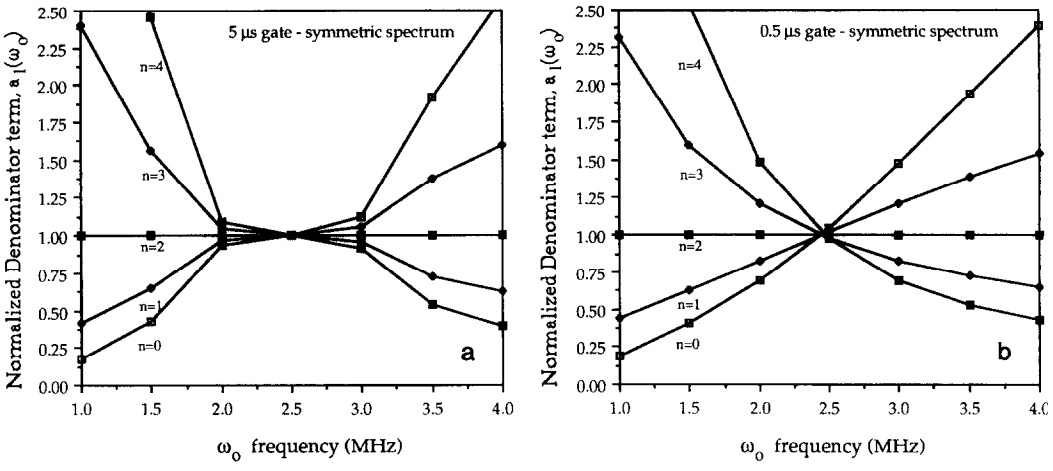

Fig. 6 Plot of the normalized $a_1(\omega_0)$ terms for a 5 μs duration time gate (a) and a 0.5 μs duration time gate (b) vs. the frequency used for ω_0. n represents the assumed amplitude frequency dependence of scattering included in the analysis. Each curve is normalized to the values calculated for n=2. Note how at the edges of the pulse spectrum (1 MHz and 4 MHz) the values for $a_1(\omega_0)$ vary widely, especially for the 0.5 μs gate analysis. At 2.5 MHz (the center of the pulse) the data do not vary under different assumptions regarding the scattering dependency on frequency.

The frequency dependence of scattering is introduced in Eq. (2) via the ratio $g(\omega)/g(\omega_0)$, where ω_0 is the analysis frequency. For example, if

$$\left|\frac{g(\omega)}{g(\omega_0)}\right|^2 = \left(\frac{\omega}{\omega_0}\right)^n$$

Rayleigh scattering corresponds to n=4, while n=0 represents scattering independent of frequency.

To gain further insight into the dependence of $a_1(\omega_0)$ on $g(\omega)/g(\omega_0)$, the integral was evaluated for several analysis frequencies (ω_0). The integral was also evaluated using scattering frequency dependencies (n) ranging from zero to four. The transducer modelled was a single element focused radiator with a 19 mm aperture and a 100 mm radius of curvature. The supporting medium was tissue-like, having a speed of sound of 1540 m/s and an attenuation coefficient of 0.5 dB/cm/MHz. A 2.5 MHz center frequency pulse having a symmetric frequency distribution was assumed.

Calculated $a_1(\omega_0)$ values are shown in figure 6 for two different time gates. For convenience in plotting, the values were normalized at each analysis frequency to the value of $a_1(\omega_0)$ obtained when n=2. When the time gate is fairly long (5 μs, Fig. 6a) $a_1(\omega_0)$ is not highly dependent on the choice of n for analysis frequencies over most of the spectrum of the pulse. This is consistent with experimental results reported in table I for the 10 μs gate.

Notice in figure 6a, the values of $a_l(\omega_o)$ computed using different n converge to the same quantity within 0.5 MHz of the center frequency. This implies that the assumed functional form of $g(\omega)/g(\omega_o)$ is not critical in obtaining correct backscatter results for the 5 μs time gate. However, for the 0.5 μs time gate (Fig. 6b), $a_l(\omega_o)$ varies significantly with n at nearly every frequency, implying the $g(\omega)/g(\omega_o)$ must be known and included in the data analysis to obtain accurate results. The exception to this is when the analysis frequency is at the center frequency of the pulse, where again it is seen that all values of n yield nearly the same value of $a_l(\omega_o)$. Hence, a data analysis using this technique at the center frequency of the pulse spectrum need not include the frequency dependence of scattering.

There are two advantages to using broad-band pulses and short-duration time gate analysis in backscatter coefficient imaging. One is the obvious improvement in spatial resolution in the images, due to the smaller volumes used to determine acoustic backscatter coefficients. The second advantage is a potential improvement in the grey scale variations seen in the backscatter coefficient images. (The source of these variations is the same as "speckle" seen in B-mode images.) When the time duration of each segment τ is decreased from 3 μs to 0.5 μs, the number of statistically independent backscatter estimators in the data set increases by a factor of six. Therefore, for the same averaging volume used previously, one can average six times as many backscatter estimators and therefore reduce these variations by a factor of $\sqrt{6} = 2.45$. Additionally, one could make a series of images ranging from little or no backscatter estimator averaging and higher spatial resolution to a high degree of backscatter estimator averaging while better contrast resolution.

Increasing the number of estimators places increased demand on the computational requirements for this technique. $a_l(\omega_o)$ is the most computationally intensive equation in the data analysis. The time and

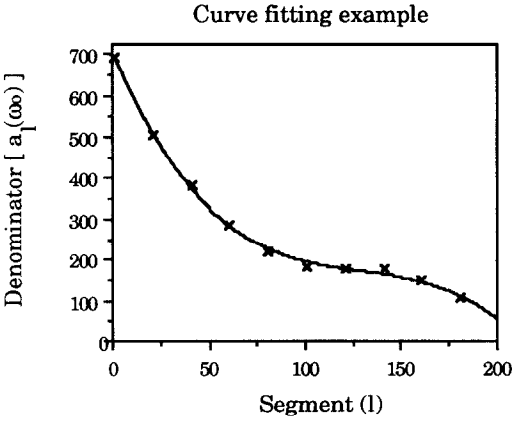

Fig. 7 An approach used to save time in the analysis of the data. If the echo signal waveform is separated into a large number of segments, the data analysis becomes undesirably long. However, since $a_l(\omega_o)$ is a smoothly varying function, one can compute a selected few and use a curve-fit to generate the remaining $a_l(\omega_o)$ terms.

computer power required can be reduced by observing that $a_l(\omega_o)$ is a smoothly varying function. One can then describe $a_l(\omega_o)$ versus l by utilizing a least squares fit to a small set of points along l. Figure 7 is a plot of the $a_l(\omega_o)$ values for a typical experiment versus the index of depth, l (which is proportional to the time following the emission of the pulse). Note that $a_l(\omega_o)$ vs. l is indeed a smoothly varying function which can be fit to a 4th or 5th order polynomial. The computation time required for determination of $a_l(\omega_o)$ can be reduced by computing, for example, 1 out of every 10 $a_l(\omega_o)$ factors. Then, using a least squares fit to these few values, $a_l(\omega_o)$ can be generated for all values of l which are required.

$a_l(\omega_o)$ could be pre-computed for any ω_o as long as the ultrasonic system has sufficiently stable transmit/receive electronics such that the $T(\omega)B_o(\omega)$ factors can be considered invariant. Computations of $a_l(\omega_o)$ could then be done for a range of attenuation coefficients over frequency ($\alpha(f)/f$) with curve fitting introduced. These $a_l(\omega_o)$ values would be stored in a look-up table and quickly accessed for use in Eq. 1 during image formation.

SUMMARY

We have applied broad-band pulses and short-duration time gate analysis to backscatter coefficient imaging. The data analysis was performed at the center frequency of symmetrical, gaussian-shaped pulses. This has resulted in higher resolution images with reduced backscatter coefficient variation in the images. Accuracy in determinations of the backscatter coefficient has not suffered.

ACKNOWLEDGMENTS

This research was supported in part by grants RO1CA39224 and RO1CA25634 from the National Institutes of Health.

REFERENCES

[1] O'Donnell, M., Quantitative volume backscatter imaging, *IEEE Trans. on Sonics and Ultrasonics SU-30*, 26-36, (1983).

[2] O'Donnell, M. and Reilly, H.F., Clinical Evaluation of the B´-scan. *IEEE Trans on Sonics and Ultrasonics, SU-32*, 450-457, (1985).

[3] Boote, E.J., Zagzebski, J.A., Madsen, E.L., Hall, T.J., Instrument-Independent Acoustic Backscatter Coefficient Imaging, *Ultrasonic Imaging 10*, 121-138, (1988).

[4] Madsen, E.L., Insana, M.F., Zagzebski, J.A., Method of data reduction for accurate determination of acoustic backscatter coefficients, *J. Acoust. Soc. Am.* 76(3), 913-923, (1984).

[5] Hall, T.J., Madsen, E.L, Zagzebski, J.A., Boote, E.J., Accurate depth-independent measurement of acoustic backscatter coefficients with focused transducers. *J. Acoust. Soc. Am.*, 85(6), 2410-2416, 1989.

[6] Ryhne, T.L., Sagar, K.B., IBR5: An optimal measurement of integrated backscatter and cyclic variation of integrated backscatter. *Ultrasonic Imaging 12* 189-204, (1990).

[7] Hall, T.J, Ph.D. Thesis, University of Wisconsin-Madison, 1988.

[8] Faran, J.J., Jr., Sound scattering by solid cylinders and spheres, *J. Acoust. Soc. Am. 23*, 405-418 (1951).